This is a repository copy of *Experimental investigation of local-flexural interactive buckling of cold-formed steel channel columns*.

White Rose Research Online URL for this paper:
http://eprints.whiterose.ac.uk/129646/

Version: Published Version
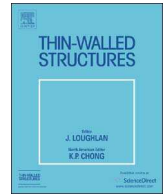
Full length article

Experimental investigation of local-flexural interactive buckling of cold-formed steel channel columns

Jun Ye[a,b], Iman Hajirasouliha[a,*], Jurgen Becque[a]

[a] Department of Civil and Structural Engineering, The University of Sheffield, Sheffield, UK
[b] College of Civil Engineering and Architecture, Zhejiang University, China

ARTICLE INFO

ABSTRACT

This paper presents the results of a comprehensive experimental programme aimed at studying the interaction of local and overall flexural buckling in cold-formed steel (CFS) plain and lipped channels under axial compression. The results were further used to verify the accuracy of the current design procedures in Eurocode 3, as well as to evaluate the effectiveness of a previously proposed optimisation methodology. A total of 36 axial compression tests on CFS channels with three different lengths (1 m, 1.5 m and 2 m) and four different cross-sections were conducted under a concentrically applied load and pin-ended boundary conditions. The initial geometric imperfections of the specimens were measured using a specially designed set-up with laser displacement transducers. Material tests were also carried out to determine the tensile properties of the flat parts of the cross-sections, as well as the cold-worked corner regions. A comparison between the experimental results and the Eurocode 3 predictions showed that the effective width approach combined with the P–M interaction equation proposed in Eurocode 3 to take into account the shift of the effective centroid consistently provided safe results. However, the Eurocode 3 procedures were also quite conservative in predicting the capacity pertaining to local-global interaction buckling, especially for plain channels. Furthermore, the experimental data confirmed the results of an optimisation study and demonstrated that the optimised CFS columns exhibited a capacity which was up to 26% higher than the standard channel with the same amount of material taken as a starting point.

1. Introduction

Cold-formed steel (CFS) structural elements have traditionally been employed as secondary load-carrying members in a wide range of applications, such as roof purlins, wall girts, stud walls and cladding. In a more recent trend, CFS elements are also increasingly being used as primary structural members, especially in low- to mid-rise multi-storey buildings [19] and portal frames with short to intermediate spans [24,25]. Compared to their hot-rolled counterparts, CFS members can potentially provide more economical and efficient design solutions due to several advantages, such as a light weight, a high flexibility in obtaining various cross-sectional shapes, a highly adaptable manufacturing process with relatively little waste, and easier and faster construction. However, as a result of the nature of the manufacturing process, CFS components are limited in wall thickness (usually to less than 6–8 mm), which makes them more susceptible to local, distortional and global buckling, as well as their interactions. Fig. 1 illustrates some of these modes for the case of a lipped channel.

The theoretical underpinnings of local-flexural interactive buckling were first established by van der Neut [36] on the basis of an idealized column made of a perfectly elastic material, which consisted only of two flanges supported along both longitudinal edges by infinitely thin webs. The importance of Van der Neut's work lies in the fact that it provided clear and important insights into the mechanics of local-overall interaction buckling and its repercussions on the column curve (indicating the column capacity as a function of the overall slenderness). The work, in combination with Van der Neut's later paper [37], also conclusively demonstrated that the sensitivity of the column capacity to both local and global imperfections becomes very pronounced when the critical stresses of both modes are of the same magnitude.

In previous experimental research Young and Rasmussen [44,45,46] investigated the ultimate capacity of plain and lipped channel CFS columns with pinned and fixed-ended boundary conditions. Their results showed that the shift of the effective centroid caused by local buckling of the column did not induce additional overall bending in fixed-ended columns, while this phenomenon was obvious in pin-ended columns. The effect of the local support conditions on the local-flexural interactive behaviour of fixed-ended plain channels was further
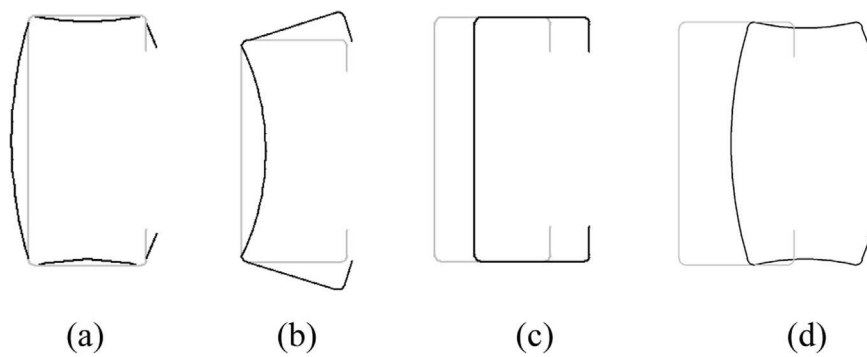
Fig. 1. Buckling modes of a lipped channel: (a) local, (b) distortional, (c) global and (d) local-flexural interactive modes.

investigated by Loughlan and Yidris [26] through numerical means. It was concluded that the plate end support conditions (either rotationally free or rotationally fixed) have a significant effect on the column behaviour, with rotationally free conditions necessary for the column to remain straight (with respect to overall flexure) above the local buckling load.

In a different study, the axial capacity of fixed-ended CFS channel columns with inclined lips was investigated experimentally and numerically by Young and Hancock [43] and Young [42]. All test specimens were observed to fail by distortional buckling. The experimental data were used to evaluate the predictions of the North-American specifications for cold-formed steel [3] and the relevant Australian/New Zealand Standard [5]. It was found that the strength predictions of the Australian/New Zealand standard were generally conservative for CFS channel columns with inclined edge stiffeners, while the North-American specifications might lead to unsafe predictions for more slender flanges. Zhang et al. [47] experimentally and numerically investigated the effect of inclined edge stiffeners on the capacity of pin-ended CFS lipped channels. Local, distortional and flexural failure modes were observed, which often occurred in combinations. The experimental results illustrated the effects of both the stiffener inclination and the load eccentricity on the failure mode and the column capacity.

Ungermann et al. [32,33,34] carried out compression test on welded plain channels made of S355 and S460. The channels were rather stocky in cross-section, with a thickness of 4 mm and depths of up to 200 mm and failed in either local or local-flexural interactive buckling. The authors also suggested improvements to the design procedure in EN1993-1-3 [15] for plain channels.

In another study a series of 36 stainless steel lipped channel columns were tested between pinned ends by Becque and Rasmussen [11]. All specimens were observed to fail in local-flexural interactive buckling. The experimental programme was followed by numerical parametric studies [12] which led to the proposal of Direct Strength design equations for stainless steel thin-walled columns [10].

More recently, CFS channel columns with intermediate V-shaped web stiffeners and return lip stiffeners were tested between pin-ended boundary conditions by Wang et al. [38]. The results of the investigation indicated that a combination of web and edge stiffeners have the potential to increase the ultimate strength of CFS channel columns by up to 70%. These results highlight the scope for optimisation research on CFS structures and the potential benefits which can be gained from developing cross-sectional shapes with improved structural capacity. An aspect of optimisation was therefore included in the research presented in this paper.

Previous optimisation research in the area of CFS has been carried out by, among others, Adeli and Karim [2], Magnucka-Blandzi [28] and Lee et al. [23,22]. Furthermore, Ma et al. [27] used Genetic Algorithms to develop optimised CFS channel cross-sections for use in compression or bending, while Ye et al. [40] used Particle Swarm Optimisation to obtain optimum CFS channel beams. In a follow-up study, Ye et al. [41] showed that more efficient cross-sections can be obtained by using

segmentally folded flanges.

The experimental work presented in this paper encompassed 36 tests on CFS channel columns, which were conducted at the Heavy Structures Laboratory at the University of Sheffield. Cross-sections obtained through the optimisation procedure previously presented by Ye et al. [40], as well as non-optimum 'standard' sections were tested in order to contrast the results. All tested specimens, however, were manufactured using the same coil width and thickness. The CFS columns were loaded concentrically using pin-ended boundary conditions and failed by the interaction of local instability and flexural buckling about the minor axis. The main aims of the experimental programme can be summarized as follows: (a) to study the interaction of local and overall flexural buckling in lipped and plain CFS channels under axial compression, (b) to verify the efficiency of the optimisation framework proposed in previous work by the authors [40] as a viable approach for more efficient design of CFS elements, and (c) to assess the accuracy of the design procedures adopted in Eurocode 3 [14–16] over a range of geometries.

2. Specimen geometry

In the design of the test specimens an optimisation framework was employed which was previously developed by the authors [40,41], which makes use of a Particle Swarm Optimisation. The total developed length of the cross-section (coil width) and the thickness (and consequently the total amount of material) were kept constant in the optimisation process. In order to apply the framework to pin-ended CFS columns, the following objective function needed to be maximized:

$$\max N_{Ed} = \left(\frac{1}{(1/N_{b,Rd})^{0.8} + (e_N/M_{b,Rd})^{0.8}} \right)^{1.25} \tag{1}$$

In the above equation $N_{b,Rd}$ and $M_{b,Rd}$ denote the member resistances in pure compression and pure bending about the minor axis, respectively, while e_N is the shift of the effective centroid caused by local/distortional buckling. The column capacity N_{Ed} thus accounts for the additional bending caused by the shift of the effective centroid, while Eq. (1) results directly from the moment-axial force interaction equation prescribed by Clause 6.2.5 of EN1993-1-3 [15].

It is noted that the calculation of the cross-sectional bending capacity $M_{b,Rd}$ in Eq. (1), based on the effective width concept, is iterative in nature. Indeed, the location of the neutral axis of the effective cross-section, which determines the stress profile over the cross-section and consequently the effective area of the web, is initially unknown. However, the Eurocode allows the designer to avoid iterations by specifying in Clause 6.1.4.1 that the stress ratio ψ (defined as the ratio of the stresses at the extremities of the web) may be based on an initial location of the neutral axis which results from accounting for the effective parts of the compression flange, but assuming the web to be fully effective. Using this ψ ratio the effective area of the web can be determined, after which the location of the neutral axis is re-calculated. After this initial iteration, further iterations are optional rather than

obligatory.

In lipped channel sections, the calculation of the pure compressive capacity $N_{b,Rd}$ is also iterative, due to the potential occurrence of distortional buckling. Clause 5.5.3.2(9) of the Eurocode specifies that, in a first step, the effective area of the lip-flange stiffener assembly may be calculated using the yield stress of the material f_y. In subsequent iterations, this stress is reduced to $\chi_d.f_y$, where the reduction factor χ_d is calculated based on the critical stress of the effective parts of the lip-flange assembly, considered as a column on an elastic foundation. However, the Eurocode clearly states that these additional iterations are again optional.

In the optimisation process described above full iterations to convergence were carried out in the determination of $M_{b,Rd}$ and $N_{b,Rd}$. The following design constraints were also considered in the optimisation process:

$$b/t \leq 60, \ c/t \leq 50, \ h/t \leq 500 \tag{2}$$

$$0.2 \leq c/b \leq 0.6 \tag{3}$$

$$c \leq 25 \tag{4}$$

where h is the cross-section depth, t is the thickness, b is the flange width and c is the lip width. Eq. (2) represent the limits on the width-to-thickness ratios set by the Eurocode (EN 1993–1-3 [15]), while Eq. (3) is imposed by Clause 5.2.2 of the Eurocode. Eq. (4) is a practical manufacturing constraint which was determined in consultation with the industrial partner of the project, who had limited flexibility in adapting the existing cold-rolling line to the production of studs with new cross-sections. While these constraints might prevent a global optimum being reached, they illustrate very well the capabilities of the previously proposed optimisation framework to incorporate various practical limitations.

The optimisation was conducted for pin-ended columns with a length $L_e = 1.5$ m. This was deemed to be the most practically relevant length as it constitutes the effective length of studs with a storey height of 3 m and one row of intermediate rods at mid-height. Additional optimisations were carried out for $L_e = 1.0$ m and $L_e = 2.0$ m and the results showed that the optimum cross-sectional dimensions did not vary significantly over these three lengths.

Four different cross-sections were considered in the test programme, of which the nominal dimensions (measured between outer surfaces) are presented in Fig. 2. All cross-sections had the same nominal thickness $t = 1.5 \ mm$ and the same total developed length (or coil width) $l = 337mm$. The four types of cross-sections were labelled A-D. Cross-section A is a standard commercially available cross-section which provided a basis for comparison. Section B is the optimum solution with the highest capacity for $L_e = 1.5$ m, subject to the constraints in Eqs. (2)–(4). Section D is a lipped channel section with an intermediate

depth relative to sections A and B and with randomly chosen dimensions, but the same coil width. Section C is a plain channel with randomly chosen dimensions, but the same coil width.

For each cross-section three different column lengths $L_e = 1.0m$, $1.5m$ and $2.0m$ were tested. In order to gain increased confidence in the results and reduce the influence of natural statistical variations in parameters such as the material properties, three columns were tested for each cross-section and length, leading to a total of 36 specimens. Tables 1–4 list the measured dimensions of the test specimens, using the nomenclature illustrated in Fig. 2. The reported dimensions are the average values of multiple measurements. The symbol r indicates the outer radius of the rounded corner, while L is the length of the column. The calculated gross cross-sectional area is denoted by A_g and is also listed in Tables 1–4. Each specimen was labelled according to its cross-section (A, B, C or D), followed by the nominal length of the column in mm and 'a', 'b' or 'c' to indicate repeat tests.

The software package CUFSM [29], which implements the finite strip method, was used to determine the critical elastic buckling stresses of each type of cross-section, as shown in Fig. 3. The local and distortional buckling stresses and their corresponding buckle half-wave lengths are listed in Table 5. It is seen that the local buckling stress is critical for all cross-sections and is always significantly smaller than the yield stress of approximately 440 MPa. It is also seen that the distortional buckling stress significantly exceeds the local buckling stress for all cross-sections. It is noted that Section C is a plain channel (see Fig. 2), for which distortional buckling does not occur. The elastic flexural (Euler) buckling stresses are also indicated in the diagrams for various column lengths. It is seen that, even for the longest columns, the Euler stress exceeds the local buckling stress, enabling local-flexural interaction. However, this interaction is expected to severely reduce the stress at which overall buckling occurs to well below the Euler stress due to the erosion of the overall bending stiffness resulting from local buckling.

3. Material properties

All specimens were manufactured using a conventional press-braking process. Tensile coupons were cut from the flat portions of all four cross-section types in order to determine their material properties (Fig. 4a). For each cross-section, one coupon was taken along the centre line of the web and another one along the centre line of the flange. In order to investigate the effect of the cold-working resulting from the manufacturing process on the material properties, coupons were also cut from the rounded corner zones. These corner coupons were tested in pairs to avoid eccentric loading (Fig. 4b). All coupons were cut from the end zones of the 1500 mm long columns after testing. The stresses during testing remained sufficiently low in these areas to justify this
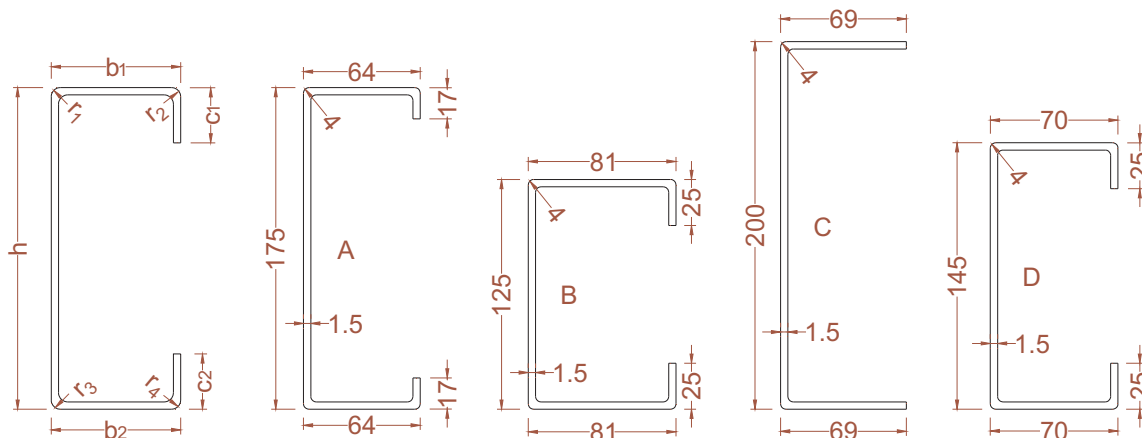

Fig. 2. Symbol definitions and nominal cross-sectional dimensions.

Table 1
Measured dimensions and calculated gross area of specimens with cross-section A.

Specimen	L (mm)	r (mm)	t (mm)	h (mm)	b_1 (mm)	c_1 (mm)	b_2 (mm)	c_2 (mm)	A_g (mm^2)
A1000-a	1000.1	4.2	1.51	174.94	64.45	17.72	64.09	18.21	485.18
A1000-b	1000.0	4.0	1.52	174.85	64.23	17.76	64.13	17.62	487.62
A1000-c	1000.0	4.1	1.50	174.89	64.27	17.82	64.12	17.51	481.16
A1500-a	1499.8	4.3	1.53	175.23	64.35	17.80	64.15	17.82	490.98
A1500-b	1500.0	4.1	1.50	174.97	63.84	18.50	63.68	17.03	480.31
A1500-c	1500.0	4.0	1.53	174.90	64.17	17.74	64.24	17.46	490.57
A2000-a	1999.8	4.1	1.52	175.62	63.86	18.86	64.09	18.11	490.28
A2000-b	2000.0	4.1	1.50	175.40	64.12	17.48	64.10	17.98	489.51
A2000-c	2000.1	4.0	1.51	175.33	64.74	18.57	64.23	16.77	486.15
Average		4.1	1.52	175.13	64.22	18.03	64.09	17.61	486.86
St. deviation		0.1	0.01	0.28	0.28	0.48	0.16	0.48	4.01

Table 2
Measured dimensions and calculated gross areas of specimens with cross-section B.

Specimen	L (mm)	r (mm)	t (mm)	h (mm)	b_1 (mm)	c_1 (mm)	b_2 (mm)	c_2 (mm)	A_g (mm^2)
B1000-a	1000.2	4.2	1.52	125.07	81.15	25.91	81.15	25.60	487.52
B1000-b	1000.0	4.0	1.52	125.19	80.74	25.69	80.74	25.31	486.24
B1000-c	1000.1	4.3	1.48	125.27	81.13	25.70	80.74	25.41	473.91
B1500-a	1500.0	4.1	1.51	125.06	81.08	26.00	80.64	25.60	483.91
B1500-b	1500.4	4.3	1.52	125.11	81.09	26.55	80.60	25.46	491.79
B1500-c	1500.1	4.0	1.53	125.24	80.74	25.94	80.88	26.51	491.79
B2000-a	2000.1	4.3	1.49	125.26	80.75	25.65	80.94	26.44	478.16
B2000-b	2000.3	4.0	1.52	125.42	81.83	26.09	81.56	24.94	489.52
B2000-c	2000.1	4.2	1.52	125.31	81.68	26.16	81.06	25.73	489.13
Average		4.2	1.51	125.22	81.13	25.96	80.92	25.67	485.77
St. deviation		0.13	0.02	0.12	0.40	0.28	0.30	0.51	6.16

Table 3
Measured dimensions and calculated gross areas of specimens with cross-section C.

Specimen	L (mm)	r (mm)	t (mm)	h (mm)	b_1 (mm)	b_2 (mm)	A_g (mm^2)
C1000-a	1000.1	4.2	1.53	199.84	69.23	69.47	504.11
C1000-b	1000.1	4.3	1.52	199.60	69.30	70.32	501.65
C1000-c	999.8	4.0	1.53	199.85	69.53	69.44	504.74
C1500-a	1500.0	4.1	1.53	199.87	69.48	70.44	506.07
C1500-b	1500.1	3.9	1.53	199.66	70.30	69.43	505.71
C1500-c	1500.2	3.8	1.52	199.90	69.83	69.53	502.42
C2000-a	2000.4	4.2	1.51	199.82	70.55	69.52	499.61
C2000-b	2000.3	4.1	1.52	199.83	70.50	69.52	502.92
C2000-c	2000.0	4.0	1.49	199.92	69.57	69.48	492.04
Average		4.1	1.50	199.80	69.80	69.70	502.14
St. deviation		0.16	0.01	0.11	0.51	0.40	4.30

procedure. The flat coupons had a gauge length of 57 mm and a width of 12.5 mm, while the corner coupons had a gauge length of 57 mm and a width of 6 mm. The coupons were tested in accordance with the specifications of the relevant European standard ISO E. 6892–1 [17]. Table 6 lists the values of the Young's modulus (E), the 0.2% stress ($\sigma_{0.2\%}$), the tensile strength (σ_u) and the elongation at fracture (ε_u)

measured over a gauge length of 50 mm. Fig. 5 also presents the measured engineering stress-strain curves and the calculated true stress-strain curves of a flat coupon (A02F) and a pair of corner coupons (B03C and B04C).

4. Imperfection measurements

The stability of thin-walled CFS members may in some cases be significantly affected by the presence of geometric imperfections, especially when coupled instabilities are involved. The magnitude and the shape of the imperfections of each specimen were therefore recorded before testing. The test set-up shown in Fig. 6 was used for this purpose. A laser was mounted on an aluminium cross beam, which was moved in the longitudinal direction of the frame at a constant speed by an electrical motor. A second electrical motor allowed the laser to move in the perpendicular direction along the aluminium beam, thus enabling the laser to cover a rectangular surface area. The laser was able to measure the distance to the surface of the test specimens with an accuracy of 0.0075 mm. The laser moved along high precision bars with minimal tolerances and its ability to maintain a level measuring plane was verified against measurements of the nominally flat table

Table 4
Measured dimensions and calculated gross areas of specimens with cross-section D.

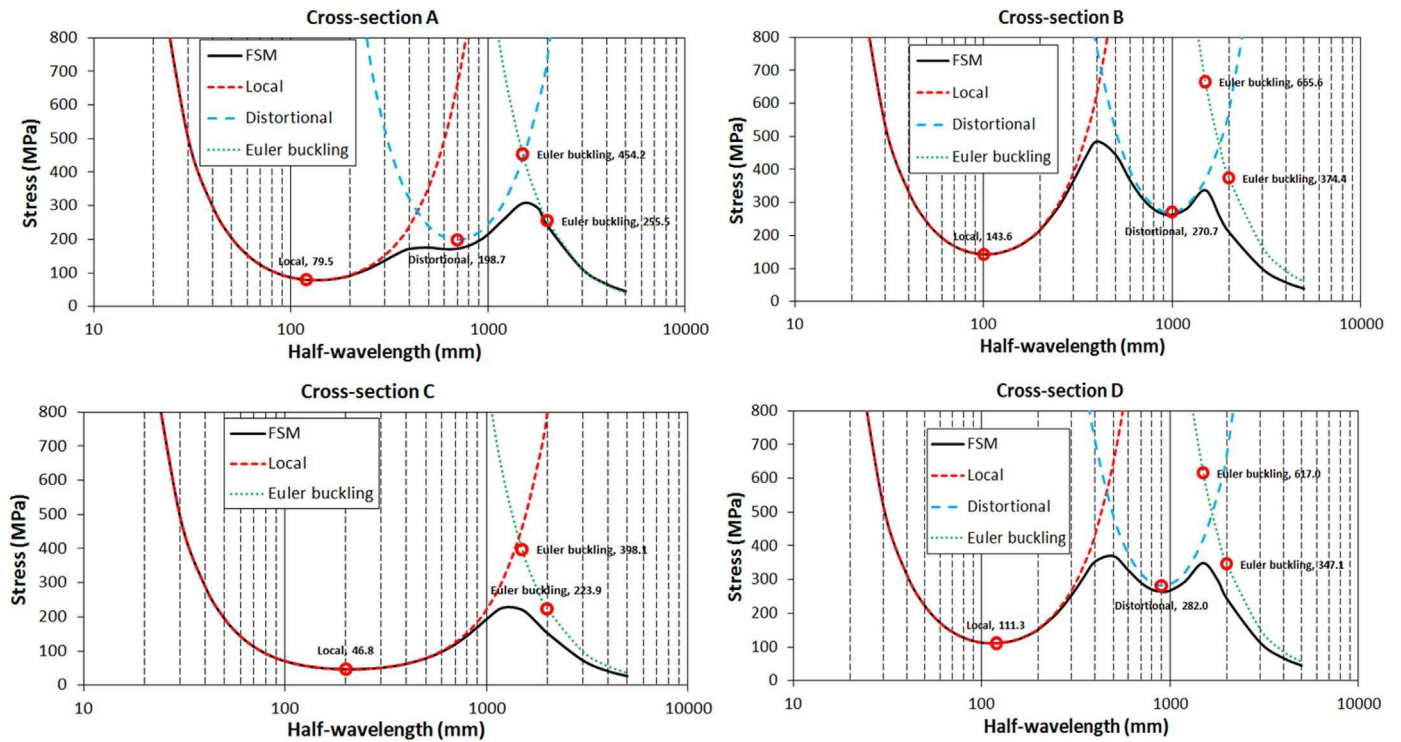| Specimen	L (mm)	r (mm)	t (mm)	h (mm)	b_1 (mm)	c_1 (mm)	b_2 (mm)	c_2 (mm)	A_g (mm^2)
D1000-a	1000.0	4.2	1.49	145.13	70.09	25.73	70.25	25.94	475.56
D1000-b	1000.2	4.1	1.51	144.90	70.43	24.60	70.47	26.82	482.18
D1000-c	1000.1	4.1	1.52	145.39	69.89	25.64	70.62	25.46	484.93
D1500-a	1500.2	4.0	1.51	145.28	69.97	25.29	70.72	25.76	482.15
D1500-b	1500.1	3.9	1.54	145.41	69.92	25.74	70.83	25.88	492.84
D1500-c	1500.0	4.2	1.52	145.34	69.92	26.01	70.62	25.87	485.78
D2000-a	2000.3	4.3	1.49	145.62	69.88	25.40	70.69	25.55	475.34
D2000-b	2000.0	4.1	1.52	145.30	69.84	25.50	70.31	26.55	485.72
D2000-c	2000.1	4.0	1.52	145.42	70.54	26.46	70.27	25.00	486.18
Average		4.1	1.5	145.30	70.10	25.6	70.50	25.90	483.41
St. deviation		0.12	0.02	0.20	0.26	0.51	0.21	0.55	5.47

Fig. 3. Signature curves obtained from CUFSM for cross-sections A, B, C and D.

Table 5
Local and distortional buckling stresses and their corresponding buckle half-wave lengths.

Sections	Buckle half-wave length (*mm*)		Buckling stress (*MPa*)		Experimental buckling stress (*MPa*)
	Local	Distortional	Local	Distortional	
A	120	700	79.5	198.7	87.1
B	100	1000	143.6	270.7	140.7
C	200	–	46.8	–	40.0
D	120	900	111.3	282.0	104.8

underneath the frame in the absence of a test specimen. This flat table was guaranteed to be grade 3, providing a surface with a deviation from flatness of less than 0.06 *mm* (BS817 2008 [13]). During the measuring process, the translational speed of the laser was set to 5 *mm/s,* while the sampling rate was 5 Hz, resulting in one reading every millimetre.

The imperfections were measured along five lines in each cross-section, as shown in Fig. 7. As an example, Fig. 8 shows the measured imperfections of specimen A2000-b along lines ① to ⑤. The readings recorded along lines ①, ② and ③ provided information about the imperfections relevant for overall flexural buckling and local buckling of the web, while the readings along lines ④ and ⑤ provided data on the imperfections affecting the distortional buckling mode. More specifically, the local imperfection was calculated by subtracting the average reading along lines ① and ③ from the readings taken along line ②. The overall imperfection was calculated as the average reading along lines ① and ③ at mid-height of the column. For the lipped channels, the distortional imperfection was equated to the maximum reading along lines ④ and ⑤. The maximum amplitudes of the recorded local, distortional and overall imperfections in the tested columns are provided in Table 7. The results indicate that the maximum out-of-plane imperfections encountered in the webs of the channels were of the order of 0.96 *mm*, while the lip-flange junctions of the lipped channels exhibited imperfections of up to 1.43 *mm*. The flange tips of the plain channels displayed out-of-plane imperfections of up to 1.60 *mm*.

5. Column tests

All 36 CFS columns (listed in Tables 1 to 4) were loaded concentrically, while using pin-ended boundary conditions about the minor
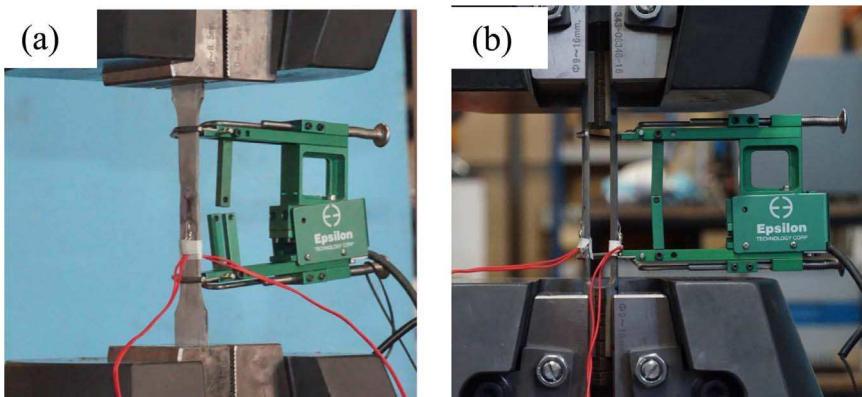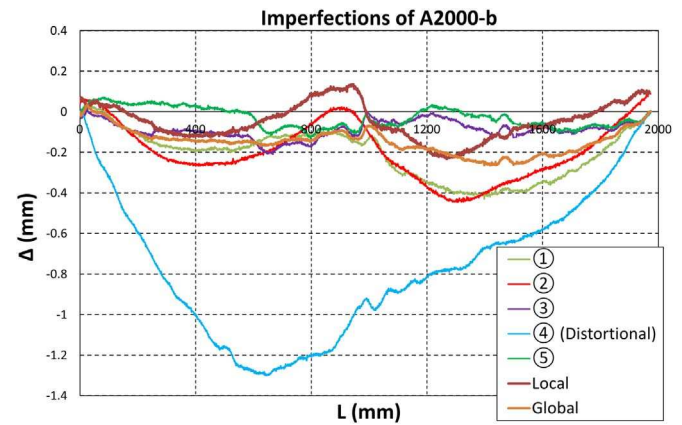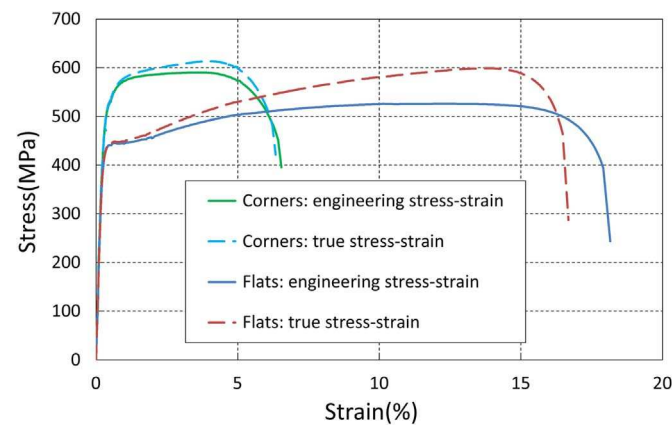

Fig. 4. Tensile material tests for: (a) flat coupons (b) corner coupons.

Table 6
Tensile properties of flat segments and corner regions.

Sections	Coupon	Type	E (MPa)	$\sigma_{0.2\%}$ (MPa)	σ_u (MPa)	ε_u (%)
A1500A	A01F	Flat	196057	447.0	524.8	18.8
	A02F	Flat	195355	448.5	525.9	18.1
	A03C	Corner	221076	525.8	591.3	6.5
	A04C					
B1500A	B01F	Flat	196194	440.3	524.9	20.1
	B02F	Flat	203486	441.2	522.1	18.2
	B03C	Corner	211164	529.6	590.5	6.5
	B04C					
C1500B	C01F	Flat	208443	453.1	531.7	18.9
	C02F	Flat	205302	459.0	533.8	20.9
	C03C	Corner	218921	530.7	579.6	6.6
	C04C					
D1500A	D01F	Flat	200226	453.9	531.8	20.7
	D02F	Flat	193743	448.5	526.0	19.3
	D03C	Corner	205742	525.6	581.1	5.9
	D04C					

Fig. 5. Stress–strain curves of the flat (A02F) and corner coupons (B03C and B04C tested as a pair).

Fig. 6. Imperfection measurement set-up.
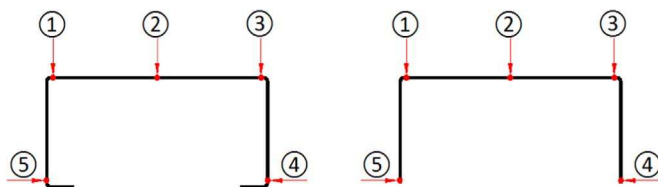
Fig. 7. Locations of the imperfection measurements.

axis. Fig. 9(a) illustrates the hinge assemblies used in the experimental set-up. The location of the minor centroidal axis was scribed onto the flanges of each specimen and the same axis was also indicated by a scribed line on the top plates of the hinge assemblies, facilitating exact

Fig. 8. Typical imperfection profile.

Table 7
Maximum amplitudes of local, distortional and overall imperfections in tested columns (in mm).

Specimen	Local	Distortional	Overall
A1000-a	0.17	0.22	0.09
A1000-b	0.24	0.14	0.12
A1000-c	0.18	0.32	0.22
A1500-a	0.18	0.38	0.37
A1500-b	0.24	0.26	0.13
A1500-c	0.27	0.41	0.06
A2000-a	0.96	0.90	0.08
A2000-b	0.23	1.30	0.07
A2000-c	0.54	1.02	0.64
B1000-a	0.29	0.38	0.02
B1000-b	0.26	0.26	0.01
B1000-c	0.27	0.28	0.02
B1500-a	0.31	0.69	0.08
B1500-b	0.29	0.46	0.18
B1500-c	0.29	0.72	0.09
B2000-a	0.26	1.03	0.14
B2000-b	0.27	1.02	0.01
B2000-c	0.22	1.03	0.47
C1000-a	0.28	0.52	0.11
C1000-b	0.19	0.63	0.04
C1000-c	0.12	0.49	0.15
C1500-a	0.22	0.74	0.07
C1500-b	0.16	0.86	0.36
C1500-c	0.27	0.78	0.19
C2000-a	0.24	1.60	0.02
C2000-b	0.19	1.57	0.47
C2000-c	0.17	1.29	0.45
D1000-a	0.21	0.31	0.04
D1000-b	0.17	0.29	0.20
D1000-c	0.22	0.34	0.11
D1500-a	0.20	0.50	0.10
D1500-b	0.22	0.62	0.28
D1500-c	0.19	0.56	0.17
D2000-a	0.31	1.43	0.13
D2000-b	0.27	0.83	0.62
D2000-c	0.18	1.04	0.04

alignment. Four steel dowels were bolted into the top plates as an additional measure in order to hold the corners of the channel in place and prevent possible slip. Fig. 9(b) shows the holes used to accommodate the dowels for the four different types of cross-sections. The distance between the horizontal axis of the hinge and the top surface of the plate was measured to be 44 *mm*. Thus, the effective length L_e of each column could be calculated by adding 88 mm to the measured specimen length L, in an approach similar to [11].

Fig. 10 illustrates the complete test set-up. A total of seven LVDTs (Linear Voltage Differential Transducers) were used to monitor the specimen displacements. The axial shortening and the end rotations of the specimens were calculated from the readings of LVDTs T1, T2, B1
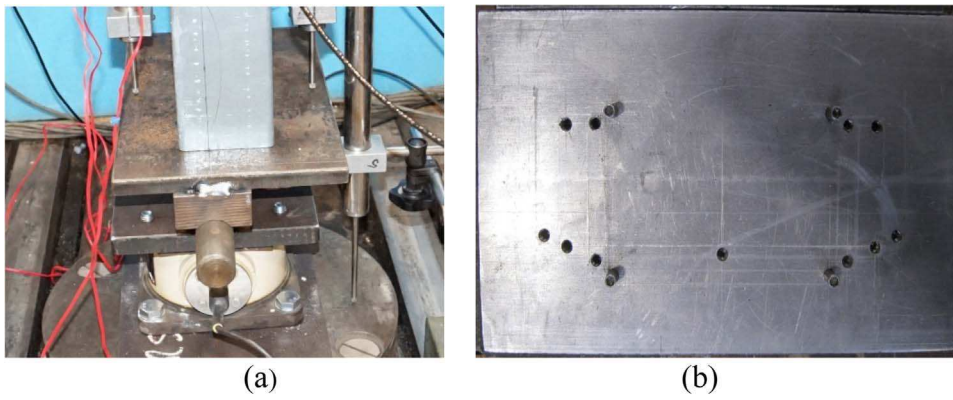
(a)   (b)

and B2. The lateral displacements at mid-height, as well as any possible twisting, were recorded by LVDTs M1 and M2. B3 was used to monitor any unexpected displacement of the base.

Previous studies (e.g. [11]) have shown that the ultimate capacity and the behaviour of CFS columns are sensitive to the value of the initial load eccentricity when local-overall interactive buckling is involved. While the test specimens in the current study were accurately positioned in the set-up with the assistance of the scribed lines and the dowels on the end plates, a select number of specimens were also instrumented with strain gauges at mid-height in order to allow an accurate verification of the initial load eccentricity. Fig. 11 shows the locations of those strain gauges, as well as the LVDTs at mid-height of the specimens. In calculating the initial load eccentricity it was assumed that the column material behaves in a linear elastic way during the initial stages of loading and that plane sections remain plane after bending. These assumptions led to the following equation for the initial load eccentricity e_0 at mid-height [9]:

$$e_0 = \frac{I_x}{A}\left(\frac{\varepsilon_1 - \varepsilon_2}{y_2\varepsilon_1 + y_1\varepsilon_2}\right) - \frac{D_1 + D_2}{2} \tag{5}$$

where ε_1 is the average reading from strain gauges SG1 and SG2, ε_2 is the average reading from strain gauges SG3 and SG4, and y_1 and y_2 are the distances from the minor centroidal axis of the section to the extreme fibres where the readings of ε_1 and ε_2, respectively, were taken. I_x and A
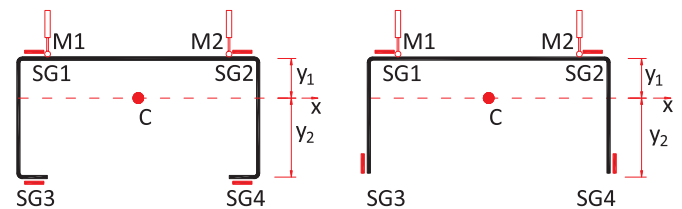
Fig. 11. Location of strain gauges and LVDTs at column mid-height.

are the second moment of area about the minor centroidal axis and the cross-sectional area, respectively. D_1 and D_2 are the lateral displacement readings from LVDTs M_1 and M_2, positioned as shown in Fig. 9. It is noted that $e_0 > 0$ indicates an eccentricity of the load towards the web.

An Amsler Universal Testing Machine with 2000 kN capacity was used to apply the compressive load, which was measured by a load cell with a range of 150 kN. The specimens were tested in a load controlled regime with a constant loading rate of 5 kN/*min*. However, the descending branch of the load-shortening curve could still be obtained through a controlled release of the hydraulic pressure at an approximate rate of 5 kN/ *min* . The experiment was terminated when the load reached less than 20% of the peak load on the descending path.

Fig. 10. Test set-up.

Fig. 12. Failure modes of 1 m long columns with type B cross-section.

6. Test results and discussion

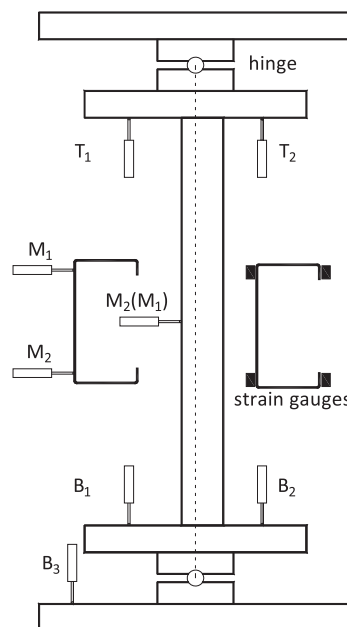All 36 specimens were observed to exhibit local buckling first, followed by eventual failure by interaction of local and overall flexural buckling about the minor axis. No distortional buckling was visually observed in any of the selected cross-sections, even at advanced stages in the post-peak behaviour. In the final stages of the tests, the local buckling deformations localized in an area near mid-height and a yield line mechanism was seen to form. Figs. 12 and 13 display the failed shapes of the 1 m long specimens with type B and C cross-sections.

Local buckling causes a shift of the effective centroid in a monosymmetric section, which consequently introduces additional bending when the column is pin-ended. In the tested lipped channel sections, the web constituted the most slender plate element in the cross-section and therefore triggered local buckling, with the effective centroid shifting away from the web. This was confirmed by the experimental observation that all lipped channel columns bent out towards their lips after buckling locally (Fig. 12). On the other hand, in the plain channels the flanges were the more slender elements, leading to a shift of the effective centroid towards the web. This was again in agreement with the experimental observation that the plain channels consistently buckled towards the web in flexure, as shown in Fig. 13.

The ultimate capacities obtained for all specimens are listed in Tables 8–11, while the measured load-shortening curves of selected columns are presented in Fig. 14. The dashed lines shown in Fig. 14 indicate the local buckling loads, as experimentally observed from the sudden change in stiffness in the load-shortening diagram. The corresponding local buckling stresses are presented in Table 5, where they are compared to the previously calculated (elastic) values. It is seen that the results compare very well and on average there is 8.5% difference between the two values.

In general, good agreement was obtained within each set of repeat

tests, with the ultimate capacities typically varying by less than 7% from the average. As an example, Fig. 15 compares the load-displacement curves of the three CFS columns with cross-section B and a nominal length of 1 m. It is seen that the different sets of experimental results agree very well over the whole load-deformation history.

Fig. 16 shows the axial load vs. the lateral displacement at mid-height of specimens A1000-a, A1000-b, A1500-a, A1500-b, A2000-a and A2000-b, as measured by LVDTs M1 and M2. The readings of both LVDTs are consistent, which indicates that the cross-sections were not subject to twisting. The diagrams in Fig. 16 indicate that the columns remained straight up to a load of approximately 45 kN. This is consistent with the load identified in Fig. 14 as the local buckling load of the Type A specimens. Fig. 16 also shows that the columns underwent increasing lateral displacements above the local buckling load, which resulted from the additional bending induced by the shift of the effective centroid.

Fig. 17 shows the strain gauges readings obtained for some of the test specimens (A1000-a, A1500-a and A2000-a). These strain gauges readings were used to determine the initial load eccentricities with the help of Eq. (5) and the results are listed in Tables 8–11 for all relevant specimens. It is seen that very consistent values were obtained within each group of cross-sections, with average values of −1.75 mm, −1.35 mm, 0.70 mm and −1.64 mm for cross-sections A, B, C and D, respectively. The consistency of these values indicates the likelihood of a small systemic error caused by an offset between the alignment tools (dowels and scribed lines) and the axis of the hinge. It can therefore be expected that the non-strain gauged specimens were subject to an initial eccentricity of similar magnitude. This initial misalignment was, however, quite small.

7. Accuracy of Eurocode 3 design procedure

The experimental data was used to evaluate the accuracy of the Eurocode 3 (EN1993-1–3 [15]) design procedures for CFS channel columns. Tables 8–11 compare the experimental results to the Eurocode 3 predictions, which were obtained using Eq. (1). As previously discussed in Section 2, an iterative procedure is needed to calculate the effective cross-sectional properties. A minimum amount of iterations is prescribed by the Eurocode, with full iterations being optional. For the sake of comparison the ultimate capacities of the specimens in this study were calculated both with full and with minimum iterations. The corresponding results are listed in Tables 8–11 as P_{u1} and P_{u2}, respectively. The actual measured dimensions and the material properties obtained from the coupon tests were used in the Eurocode calculations. Intermediate results of the calculations are presented in Table A1 in Appendix A.

The results in Tables 8–11 show that reasonable agreement was

Fig. 13. Failure modes of 1 m long columns with type C cross-section.

Table 8
Ultimate capacities of specimens with cross-section A.

Specimen	Eccentricity e_0 (mm)	Tested capacity P_u (kN)	EC3 with full iterations P_{u1} (kN)	Shift of effective centroid e_1 (mm)	EC3 with minimum iterations P_{u2} (kN)	Shift of effective centroid e_2 (mm)	P_{u1}/P_u	P_{u2}/P_u
A1000-a	−1.74	99.8	78.5	2.7	78.5	2.7	0.78	0.78
A1000-b	X	98.3	79.4	2.4	79.3	2.4	0.81	0.81
A1000-c	X	98.7	77.8	2.3	77.7	2.3	0.79	0.79
A1500-a	−1.86	95.1	71.5	2.5	71.4	2.5	0.75	0.75
A1500-b	X	85.3	68.9	2.5	68.8	2.5	0.81	0.81
A1500-c	X	91.4	71.6	2.3	71.5	2.3	0.78	0.78
A2000-a	−1.63	78.4	59.6	2.9	59.6	2.9	0.76	0.76
A2000-b	X	75.8	58.7	2.4	58.6	2.4	0.77	0.77
A2000-c	X	88.8	59.8	2.3	59.8	2.3	0.67	0.67
Average							0.77	0.77
St. Dev.							0.04	0.04

achieved between the experimentally obtained and the Eurocode predicted capacities of the lipped channel columns, with the ratio of the Eurocode predicted values to the test results ranging from 0.67 to 0.89. The average value was 0.81 with a standard deviation of 0.05. It is also seen that little additional accuracy was achieved by conducting full iterations, with the results obtained after the minimum amount of iterations differing by 2% on average from the final results. This can be attributed to the fact that the flanges of a lipped channel, when subject to a stress gradient under minor axis bending, are typically fully effective due to their limited width-to-thickness ratios. Therefore, no iterations were required in the determination of $M_{b,Rd}$. At the same time, fairly accurate values of the distortional reduction factor χ_d were obtained in the first iteration, with subsequent iterations converging fast. The predicted shift of the effective centroid did also not change substantially after the initial iteration.

It is noted that the Eurocode 3 equations predicted a small shift of the effective centroid *towards* the web in the lipped channels of type B. This was contradicted by the experiment where, despite the fact that this shift would have been compounded by the initial load eccentricity, all channels of type B were observed to bend out towards the lips. This can be explained by the fact that the calculated shift towards the web was in large part due to a predicted loss of effective area in the flange-lip assembly due to distortional buckling, while no distortional buckling was observed in the experiment. This contradiction can be explained by the fact that the Eurocode requires the effective cross-section to be calculated at the yield stress, rather than at the actual stress level. The occurrence of local-flexural interactive buckling pre-empted the critical distortional buckling stress level from being reached in the actual tests. The direction of the predicted shift in channels B also implied that the minor axis bending capacity $M_{b,Rd}$ had to be calculated assuming first yield to occur in the lips in compression, according to Clause 6.1.4.1 of EN1993-1–3 [15], using a linear stress diagram over the cross-section. In channels A and D, on the other hand, first yield occurred in the lips in tension and the inelastic reserve capacity of the cross-section,

calculated according to Clause 6.1.4.2, was taken into account.

While reasonable predictions were obtained for the lipped channels, it is seen from Table 10 that the Eurocode 3 predictions were extremely conservative for plain channel sections (type C), for which the average ratio of the predicted values to the test results was only 0.38. This can mainly be attributed to the fact that the Eurocode requires the effective cross-section to be calculated at the yield stress, rather than at the actual stress level as is common in other design standards, most notably the North-American specifications [4] and the Australian/New Zealand standards AS/NZS 4600 [6]. While both approaches generally lead to comparable results for lipped channels, cross-sections with outstand elements (such as plain channels) may be disproportionately penalized by the requirement to calculate the effective cross-section at the yield stress, since an increased loss of effective area in the flanges results in a comparatively large loss of second moment of area about the weak axis and, consequently, minor axis bending capacity. In an attempt to improve the predictions, Annex E of EN1993-1–5 [16] was invoked, which allows the effective area to be calculated at the actual stress level σ_{com}, rather than at the yield stress f_y. The stress σ_{com} thereby (conservatively) needs to be taken as the maximum stress caused by the combination of actions (compression and bending) on the effective areas (Clause 4.4(4) of EN1993-1–5 [16]). The calculations are iterative in nature and were carried out to full convergence. The results are listed as P_{u3} in Table 10. This approach improved the Eurocode predictions to, on average, 76% of the test results, with a standard deviation of 0.08. The intermediate calculation results presented in Table A1 (Appendix A) show that calculating the effective area at the actual stress level has a dramatic influence on the value of the minor axis bending capacity $M_{c,Rd}$, typically doubling its value, while it has a much more modest effect on the pure column capacity $N_{b,Rd}$. This confirms the abovementioned reasons for the conservatism of the Eurocode in predicting the capacity of plain channel columns.

It is worth noting that yet another alternative design approach is available for plain channels in EN1993-1–3 [15] by invoking Annex D

Table 9
Ultimate capacities of specimens with cross-section B.

Specimen	Eccentricity e_0 (mm)	Tested capacity (kN)	EC3 with full iterations P_{u1} (kN)	Shift of effective centroid e_1 (mm)	EC3 with minimum iterations P_{u2} (kN)	Shift of effective centroid e_2 (mm)	P_{u1}/P_u	P_{u2}/P_u
B1000-a	X	113.8	98.3	−1.0	104.2	−0.3	0.86	0.92
B1000-b	−1.27	110.3	98.1	−1.0	104.2	−0.3	0.89	0.94
B1000-c	X	107.7	92.2	−1.3	98.2	−0.5	0.86	0.91
B1500-a	−1.34	103.8	89.5	−1.1	94.7	−0.4	0.86	0.91
B1500-b	X	107.9	91.0	−1.1	96.1	−0.4	0.84	0.89
B1500-c	X	106.2	92.1	−1.1	97.3	−0.4	0.87	0.92
B2000-a	−1.44	99.6	78.7	−1.3	82.9	−0.5	0.79	0.83
B2000-b	X	101.6	81.9	−1.2	86.2	−0.5	0.81	0.85
B2000-c	X	105.3	82.0	−1.2	86.3	−0.5	0.78	0.82
Average							0.84	0.89
St. Dev.							0.04	0.04

Table 10
Ultimate capacities of specimens with cross-section C.

Specimen	Eccentricity e_0 (mm)	Tested capacity (kN)	EC3 with full iterations P_{u1} (kN)	Shift of effective centroid e_1 (mm)	EC3 at actual stress level P_{u3} (kN)	Shift of effective centroid e_3 (mm)	P_{u1}/P_u	P_{u3}/P_u
C1000-a	X	33.6	14.8	−10.0	26.3	−8.6	0.44	0.78
C1000-b	+0.79	43.8	14.4	−10.2	25.5	−8.8	0.33	0.58
C1000-c	X	42.7	14.7	−10.1	26.2	−8.6	0.34	0.61
C1500-a	+0.68	36.3	14.0	−10.2	26.5	−8.5	0.38	0.73
C1500-b	X	35.2	13.9	−10.2	26.5	−8.5	0.40	0.75
C1500-c	X	37.1	13.7	−10.2	26.1	−8.4	0.37	0.70
C2000-a	+0.63	33.1	12.7	−10.3	26.2	−8.1	0.38	0.79
C2000-b	X	31.7	12.9	−10.3	26.7	−8.0	0.41	0.84
C2000-c	X	33.8	12.3	−10.2	25.6	−8.0	0.37	0.76
Average							0.38	0.73
St. Dev.							0.03	0.08

Table 11
Ultimate capacities of specimens with cross-section D.

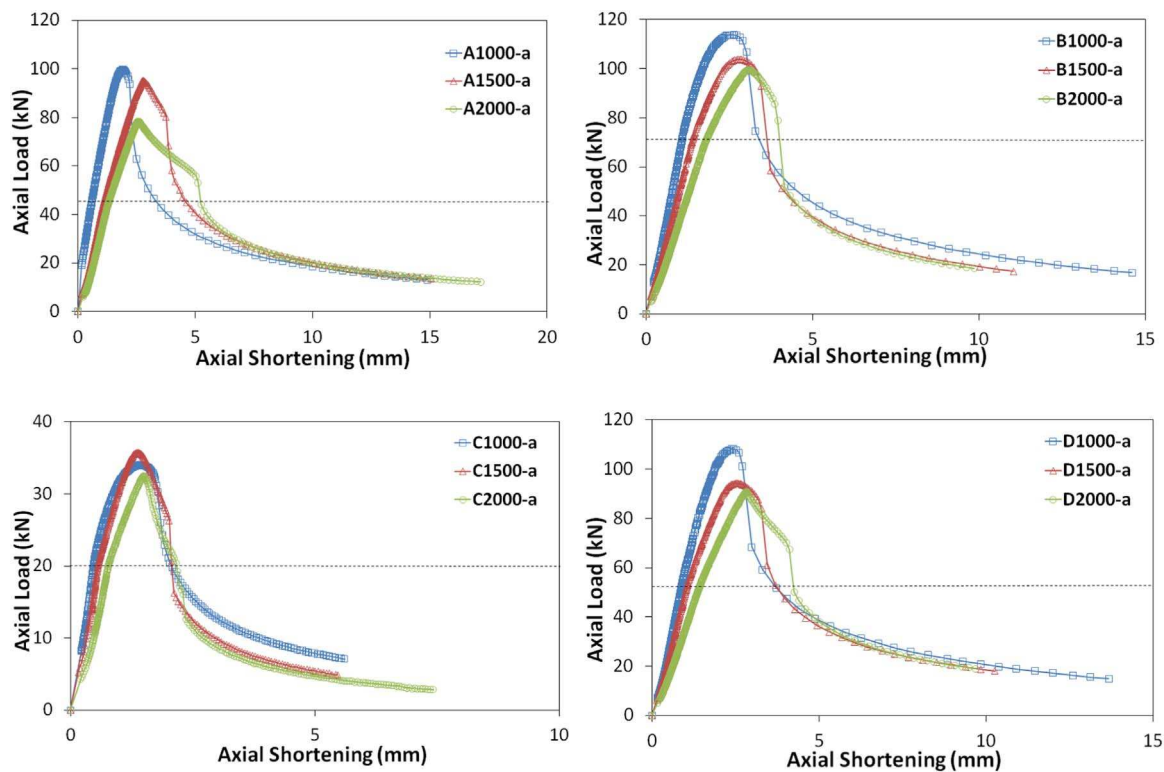| Specimen	Eccentricity e_0 (mm)	Tested capacity (kN)	EC3 with full iterations P_{u1} (kN)	Shift of effective centroid e_1 (mm)	EC3 with minimum iterations P_{u2} (kN)	Shift of effective centroid e_2 (mm)	P_{u1}/P_u	P_{u2}/P_u
D1000-a	X	109.0	90.1	1.9	89.3	2.4	0.83	0.82
D1000-b	X	110.8	92.3	1.9	91.6	2.3	0.83	0.83
D1000-c	−1.81	109.3	92.8	2.0	92.1	2.4	0.85	0.84
D1500-a	−1.49	95.0	83.7	1.9	83.0	2.3	0.88	0.87
D1500-b	X	98.2	86.3	2.1	85.6	2.5	0.88	0.87
D1500-c	X	99.6	84.4	2.0	84.4	2.0	0.85	0.85
D2000-a	X	90.8	71.4	1.8	70.8	2.3	0.79	0.78
D2000-b	−1.63	97.8	73.4	2.1	72.8	2.5	0.75	0.74
D2000-c	X	89.6	73.8	2.0	73.2	2.4	0.82	0.82
Average							0.83	0.82
St. Dev.							0.04	0.04

Fig. 14. Axial load versus end shortening curves of 'a' series specimens.

to calculate the effective cross-section of outstand elements. The above conclusions regarding plain channels agree well with previous work by Young and Rasmussen [46] who concluded that the effective width concept leads to conservative predictions for pin-ended plain channels undergoing local-flexural interaction, a fact which they attributed to the shift of the effective centroid being overestimated by the design standards relative to the experimentally measured values. This has encouraged other researchers [21,34] to propose modifications to the
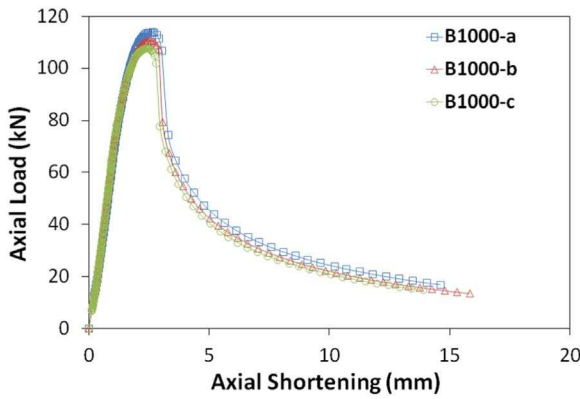
Fig. 15. Comparison of axial load versus end shortening curves of specimens with cross-section B and nominal length of 1 m.

Eurocode 3 design approach for plain channels.

8. Evaluation of the optimisation process

The experimental results also allowed an evaluation of the

efficiency of the optimisation framework previously presented in [40]. While section A is a standard commercially available cross-section and sections C and D are additional non-optimum solutions, section B is the lipped channel with the highest compressive capacity subject to the design and manufacturing constraints presented in Eqs. (2)–(4). It is seen from Tables 8–11 that the experiments confirm the optimisation results and demonstrate that the channel B offers a considerably higher compressive capacity, with average increases of 18% and 7% over specimens A and D, respectively.

9. Direct strength method

The Direct Strength Method (DSM) provides an alternative design method to the effective width concept. It has seen a lot of development and gain in acceptance over the past few decades. The method found its origins in work by Hancock et al. [20] on the distortional buckling mode, but was further developed into the currently established form by Schafer and Peköz [31]. Although it is presently not supported by the Eurocode provisions, the DSM has been included in the North-American ([4] – Appendix 1) and Australian/New Zealand [6] design standards for cold-formed steel structural members. An alternative form of a direct design method based on similar principles, called the Effective
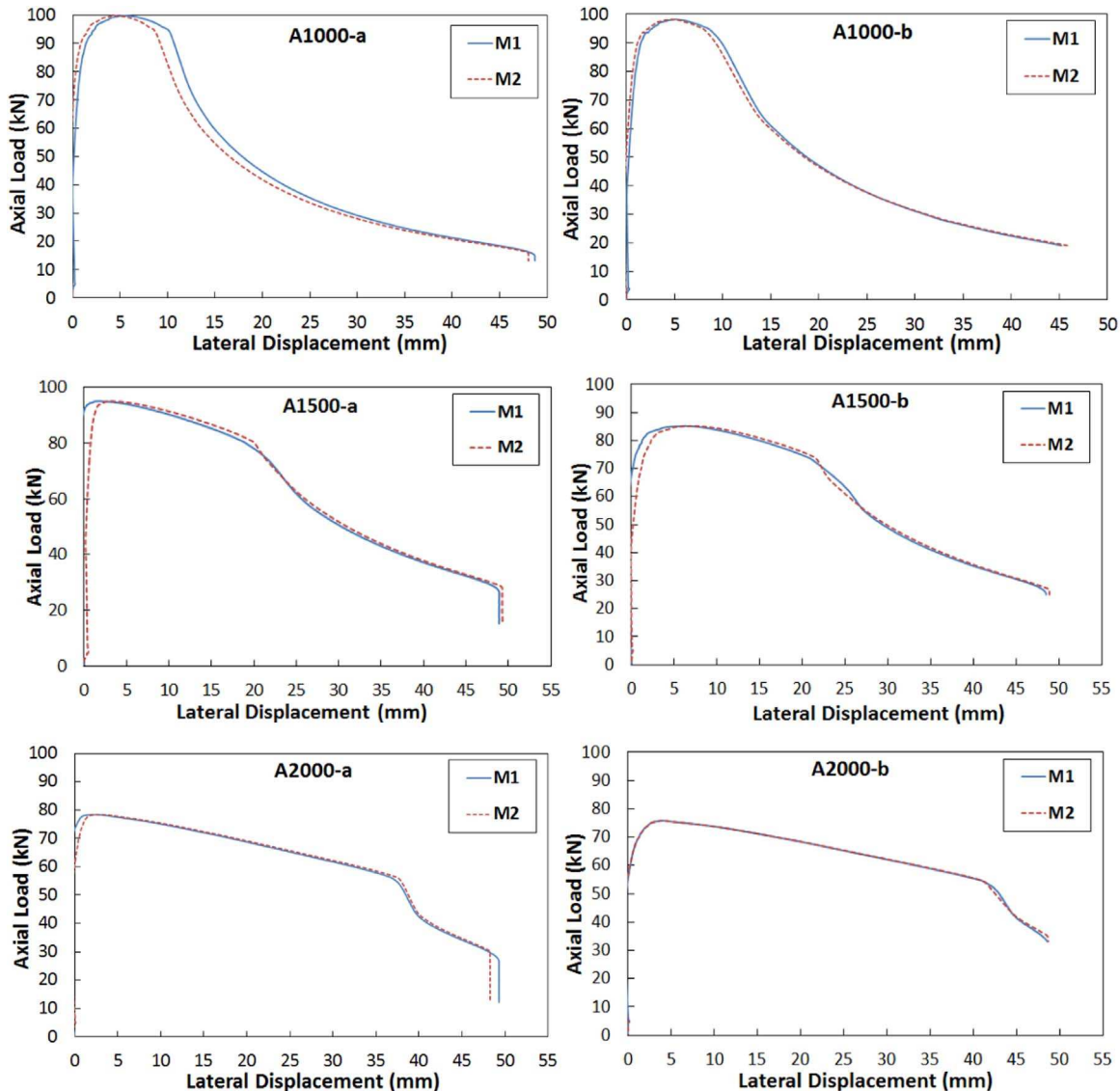

Fig. 16. Axial load vs. lateral displacement at mid-height of specimens A1000-a, A1000-b, A1500-a, A1500-b, A2000-a and A2000-b.
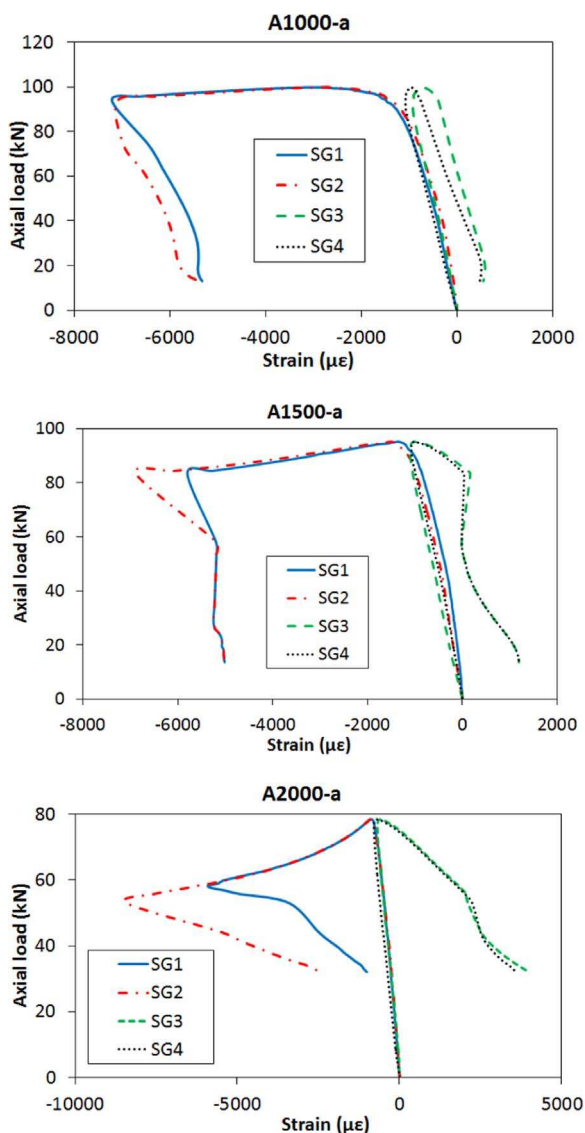
Fig. 17. Axial load versus measured strain (specimens A1000-a, A1500-a and A2000-a).

qualified, while plain channels are not.

The test results presented in Section 5 were compared to the predictions of the DSM equations presented in the North-American and Australian/New Zealand standards. The freely available software tool CUFSM [35] was used to calculate the elastic buckling stresses for the local and distortional modes. The DSM resulted in an average ratio of predicted to experimental capacity of 0.95 with a standard deviation of 0.081 over the range of lipped channels A, B and D. Detailed results can be found in [39]. The DSM thus outperformed the EC3 design rules, which over the same data resulted in a ratio of predicted to experimental capacity of 0.81 with a standard deviation of 0.051.

10. Conclusions

A total of 36 CFS channel column tests, including four different cross-sectional geometries and three different lengths, were carried out with the aim of (a) investigating the interaction of the local and overall flexural buckling modes, (b) verifying the accuracy of the relevant Eurocode 3 design procedures, and (c) assessing the efficiency of a practical optimisation framework developed in previous studies. The specimens were tested under a nominally concentric load between pin-ended boundary conditions. The geometric imperfections were measured with laser displacement transducers using a specially designed set-up. Material tests were also carried out to determine the properties of the flat segments and the rounded corner regions of each cross-section type. Based on an analysis of the results, the following conclusions could be drawn:

(1) The experiments were successful in achieving interaction between local buckling and flexural buckling about the minor axis. Good agreement was obtained within each set of three nominally identical tests, with the ultimate loads differing by less than 7% from the average.
(2) Additional overall bending of the specimens, resulting from a shift of the effective centroid, was observed after the appearance of a local buckling pattern. Bending consistently occurred towards the web in the plain channels and towards the lips in the lipped channels.
(3) The Eurocode 3 design procedures provided conservative predictions of the ultimate capacities of the pin-ended lipped channel columns, with an average ratio of the Eurocode predicted values to the test results of 0.81 and a standard deviation of 0.05. However, the Eurocode 3 predictions were extremely conservative for the plain channel columns, with an average ratio of the predicted to the measured capacities of just 0.38. The predictions were significantly improved by invoking Annex E of EN1993-1–5 [16] and calculating the effective cross-section using the actual stress level, rather than the yield strength.
(4) The ultimate capacities of the optimised CFS columns measured in the experiments were on average 19% higher than the capacities of the commercially available lipped channel with the same amount of material which was taken as a starting point. The results thus demonstrate the effectiveness and reliability of the previously proposed optimisation model [40] in improving the compressive capacity of CFS structural members and prove that the method can provide a practical tool for manufacturers and structural engineers.

Section Method, was developed by Batista [7,8] and has been included in the Brazilian code [1]. The DSM can be seen as an extension of conventional column design for global buckling in that a slenderness parameter is defined for the local and distortional buckling modes based on the yield stress and the elastic buckling stress of the particular mode. Explicit expressions, analogous to the column buckling curves, are then used to directly provide the capacity. It should be noted that the DSM in its current form also accounts for local-global interaction by replacing the yield stress in the definition of the local slenderness by the inelastic column buckling stress. The DSM is straightforward in its principles and application, avoiding the calculation of effective section properties, which can be tedious for complex cross-sectional shapes including stiffeners. However, it requires an elastic stability analysis to be carried out as part of the design process, for which freely or commercially available software tools typically based on the Finite Strip Method [18] or Generalized Beam Theory [30] can be used. Since the DSM is in essence a statistical method which requires validation of the proposed design equations against experimental and numerical data, it relies on the concept of pre-qualified sections. Section geometries which have not been included in the calibration of the design equations (and are thus not pre-qualified) consequently need to be designed with a higher safety factor [4]. Lipped channels without stiffeners are pre-

Appendix A

See Table A1

Table A1
Predicted capacities according to the Eurocode: intermediate results.

Specimen	Full iterations					Minimum iterations				
	A_{eff}	$\overline{\lambda}$	χ	$N_{b,Rd}$	$M_{c,Rd}$	A_{eff}	$\overline{\lambda}$	χ	$N_{b,Rd}$	$M_{c,Rd}$
-	(mm^2)	-	-	(kN)	(kNm)	(mm^2)	-	-	(kN)	(kNm)
A1000-a	230	0.474	0.896	92.0	2.80	229	0.473	0.896	91.9	2.80
A1000-b	231	0.476	0.895	92.6	2.81	231	0.475	0.895	92.4	2.81
A1000-c	225	0.473	0.896	90.4	2.76	225	0.472	0.896	90.2	2.76
A1500-a	235	0.696	0.786	82.5	2.84	234	0.696	0.786	82.4	2.84
A1500-b	226	0.696	0.786	79.5	2.73	226	0.696	0.786	79.4	2.73
A1500-c	233	0.696	0.786	82.2	2.83	233	0.695	0.786	82.1	2.83
A2000-a	235	0.916	0.651	68.5	2.83	235	0.915	0.651	68.4	2.83
A2000-b	226	0.908	0.656	66.2	2.76	225	0.908	0.656	66.2	2.76
A2000-c	228	0.904	0.659	67.2	2.80	227	0.903	0.659	67.1	2.80
B1000-a	256	0.373	0.936	105.5	3.71	261	0.377	0.935	107.5	3.71
B1000-b	255	0.373	0.937	105.4	3.71	260	0.377	0.935	107.4	3.71
B1000-c	242	0.367	0.939	100.2	3.60	248	0.371	0.937	102.3	3.60
B1500-a	252	0.541	0.866	96.2	3.69	258	0.547	0.863	98.0	3.69
B1500-b	256	0.543	0.865	97.5	3.72	261	0.549	0.862	99.2	3.72
B1500-c	259	0.543	0.865	98.8	3.76	265	0.549	0.862	100.5	3.76
B2000-a	246	0.706	0.780	84.6	3.63	251	0.714	0.776	86.0	3.63
B2000-b	255	0.705	0.781	87.7	3.78	260	0.713	0.776	89.1	3.78
B2000-c	256	0.708	0.779	87.8	3.76	261	0.715	0.775	89.2	3.76
C1000-a	146	0.420	0.887	59.1	0.243	199	0.491	0.848	77.3	0.448
C1000-b	144	0.415	0.889	58.6	0.239	197	0.484	0.852	76.5	0.438
C1000-c	146	0.418	0.888	59.1	0.243	200	0.489	0.849	77.3	0.447
C1500-a	146	0.605	0.782	52.2	0.243	211	0.727	0.708	68.0	0.497
C1500-b	146	0.606	0.782	52.1	0.243	211	0.728	0.707	68.0	0.497
C1500-c	144	0.606	0.782	51.4	0.238	208	0.728	0.707	67.1	0.488
C2000-a	143	0.790	0.668	43.5	0.235	224	0.991	0.545	55.8	0.568
C2000-b	144	0.793	0.667	43.9	0.239	228	0.995	0.543	56.3	0.581
C2000-c	139	0.792	0.667	42.2	0.225	220	0.996	0.542	54.3	0.550
D1000-a	246	0.428	0.915	101.6	3.39	250	0.432	0.913	103.1	3.39
D1000-b	252	0.429	0.914	104.0	3.47	256	0.432	0.913	105.5	3.47
D1000-c	255	0.432	0.913	105.1	3.48	259	0.435	0.912	106.6	3.48
D1500-a	252	0.627	0.823	93.5	3.46	256	0.632	0.821	94.7	3.46
D1500-b	262	0.632	0.821	97.1	3.57	266	0.637	0.818	98.3	3.57
D1500-c	256	0.630	0.822	95.0	3.49	260	0.635	0.819	96.1	3.49
D2000-a	245	0.821	0.712	78.7	3.38	249	0.828	0.707	79.5	3.38
D2000-b	257	0.831	0.705	81.7	3.48	260	0.837	0.702	82.4	3.48
D2000-c	255	0.826	0.708	81.7	3.50	259	0.832	0.704	82.4	3.50

EN1993-1-5 Annex E

.

References

[1] ABNT NBR 14762, *Steel structures, design of cold-formed members*. Associação Brasileira de Normas Técnicas (in Portuguese), 2010.

[2] H. Adeli, A. Karim, Neural network model for optimization of cold-formed steel beams, *J. Struct. Eng.,* ASCE 123 (1997) 1535–1543.

[3] AISI, North American Cold-formed Steel Specification: Specification for the Design of Cold-formed Steel Structural Members, American Iron and Steel Institute, Washington, DC, USA, 2001.

[4] AISI, North American Specification for the Design of Cold-formed Steel Structural Members, American Iron and Steel Institute, Washington, DC, USA, 2016.

[5] AS/NZS, AS/NZS 4600: Cold-formed Steel Structures, Joint Technical Committee BD-082, Sydney, Australia, 1996.

[6] AS/NZS, AS/NZS 4600: cOld-formed Steel Structures, Joint Technical Committee BD-082, Sydney, Australia, 2005.

[7] E.M. Batista, Etude de la stabilité des profils à parois minces et section ouverte de types U et C. Collection des publications de la Faculté des Sciences Appliquées no. 119, University of Liège, 1989.

[8] E.M. Batista, Effective section method: a general direct method for the design of steel cold-formed members under local-global buckling interaction, Thin-Walled Struct. 48 (2010) 345–356.

[9] J. Becque, The Interaction of Local and Overall Buckling of Cold-formed Stainless Steel Columns, Ph.D. Thesis The University of Sydney, Sydney, Australia, 2008.

[10] J. Becque, M. Lecce, K.J.R. Rasmussen, The Direct Strength Method for stainless steel compression members, J. Constr. Steel Res. 64 (11) (2008) 1231–1238.

[11] J. Becque, K.J.R. Rasmussen, Experimental investigation of local-overall interaction buckling of stainless steel lipped channel columns, J. Constr. Steel Res. 65 (8–9) (2009) 1677–1684.

[12] J. Becque, K.J.R. Rasmussen, A numerical investigation of local-overall interaction buckling of stainless steel lipped channel columns, J. Constr. Steel Res. 65 (8–9) (2009) 1685–1693.

[13] British Standards, BS817: Specification for surface plates, UK, 2008.

[14] CEN, EN1993-1-1 Eurocode3: Design of steel structures, Part 1.1: General rules and rules for buildings. European Committee for Standardization, Brussels, 2005.

[15] CEN, EN1993-1-3 Eurocode 3: Design of steel structures, Part 1.3: Supplementary rules for cold formed members and sheeting. European Committee for Standardization, Brussels, 2006.

[16] CEN, EN1993-1-5 Eurocode 3: Design of Steel Structures, part 1-5: Plated structural elements. European Committee for Standardization, Brussels, 2006.

[17] CEN, ISO E. 6892-1 Metallic materials; Tensile testing Part 1: Method of test at room temperature. CEN Brussels. 2009, 2009.

[18] Y.K. Cheung, Finite Strip Method in Structural Analysis, Pergamon Press, New York, 1976.

[19] L. Fiorino, O. Iuorio, R. Landolfo, Designing CFS structures: the new school BFS in Naples, Thin-Walled Struct. 78 (2014) 37–47.

[20] G.J. Hancock, Y.B. Kwon, E.S. Bernard, Strength design curves for thin-walled sections undergoing distortional buckling, J. Constr. Steel Res. 31 (2–3) (1994) 169–186.

[21] J. Kalameya, Zur Tragfähigkeit von Druck- und Biegebeanspruchten C-Profilen aus Stahl, Ph.D. Thesis University of Technology, Dortmund (in German), 2008.

[22] J. Lee, S.-M. Kim, H.-S. Park, Optimum design of cold-formed steel columns by using micro genetic algorithms, Thin-Walled Struct. 44 (2006) 952–960.

[23] J. Lee, S.-M. Kim, H.-S. Park, B.-H. Woo, Optimum design of cold-formed steel channel beams using micro Genetic Algorithm, Eng. Struct. 27 (2005) 17–24.

[24] J.B.P. Lim, D.A. Nethercot, Ultimate strength of bolted moment-connections between cold-formed steel members, Thin-Walled Struct. 41 (2003) 1019–1039.

[25] J.B.P. Lim, D.A. Nethercot, Finite element idealization of a cold-formed steel portal frame, J. Struct. Eng., ASCE 130 (2004) 78–94.

[26] J. Loughlan, N. Yidris, The local-overall flexural interaction of fixed-ended plain channel columns and the influence on behaviour of local conditions at the constituent plate ends, Thin-Walled Struct. 81 (2014) 132–137.

[27] W. Ma, J. Becque, I. Hajirasouliha, J. Ye, Cross-sectional optimization of cold-formed steel channels to Eurocode 3, Eng. Struct. 101 (2015) 641–651.

[28] E. Magnucka-Blandzi, Effective shaping of cold-formed thin-walled channel beams with double-box flanges in pure bending, Thin-Walled Struct. 49 (2011) 121–128.

[29] B. Schafer. CUFSM software Version 3.12. Department of Civil Engineering, Johns Hopkins University, USA. ⟨http://www.ce.jhu.edu/bschafer/cufsm/⟩.

[30] R. Schardt, Verallgemeinierte technische biegetheorie (Generalised beam theory), Springer Verlag, Berlin, Heidelberg, 1989.

[31] B.W. Schafer, T. Peköz. Direct Strength Prediction of Cold-Formed Steel Members using Numerical Elastic Buckling Solutions. Proceedings of the 14th International Specialty Conference on Cold-Formed Steel Structures, St. Louis, Missouri, 69 − 76.

[32] D. Ungermann, B. Brune, S. Lübke, Experimental investigations on plain channels in coupled instabilities, Steel Constr. 5.2 (2012) 87–92.

[33] D. Ungermann, B. Brune, S. Lübke, Numerical and analytical investigations on plain channels in coupled instabilities, Steel Constr. 5.4 (2012) 205–211.

[34] D. Ungermann, S. Lübke, B. Brune, Tests and design approach for plain channels in local and coupled local-flexural buckling based on eurocode 3, Thin-walled Struct. 81 (2014) 108–120.

[35] B.W. Schafer, S. Adany, Buckling analysis of cold-formed steel members using CUFSM: conventional and constrained finite strip methods. Proceedings of the eighteenth international specialty conference on cold-formed steel structures, Orlando, USA, 2006.

[36] A. van der Neut, The interaction of Local Buckling and Column Failure of Thin-walled Compression Members, Proc. 12th Int. Congr. Appl. Mech. (1969) 389–399.

[37] A. van der Neut, The Sensitivity of Thin-walled Compression Members to Column Axis Imperfection, Int. J. Solids Struct. 9 (1973) 999–1011.

[38] C.A. Wang, Z.N. Zhang, D.Q. Zhao, Q.Q. Liu, Compression tests and numerical analysis of web-stiffened channels with complex edge stiffeners, J. Constr. Steel Res. 116 (2016) 29–39.

[39] J. Ye, More Efficient Cold-formed Steel Elements and Bolted Connections, Ph.D. Thesis The University of Sheffield, Sheffield, UK, 2016.

[40] J. Ye, I. Hajirasouliha, J. Becque, A. Eslami, Optimum design of cold-formed steel beams using particle swarm optimization method, J. Constr. Steel Res. 122 (2016) 80–93.

[41] J. Ye, I. Hajirasouliha, J. Becque, K. Pilakoutas, Development of more efficient cold-formed steel channel sections in bending, Thin-walled Struct. 101 (2016) 1–13.

[42] B. Young, Design of channel columns with inclined edge stiffeners, J. Constr. Steel Res. 60 (2004) 183–197.

[43] B. Young, G.J. Hancock, Compression tests of channels with inclined simple edge stiffeners, J. Struct. Eng., ASCE 129 (2003) 1403–1411.

[44] B. Young, K.J.R. Rasmussen, Tests of fixed-ended plain channel columns, J. Struct. Eng., ASCE 124 (2) (1998) 131–139.

[45] B. Young, K.J.R. Rasmussen, Behaviour of cold-formed singly symmetric columns, Thin-Walled Struct. 33 (1999) 83–102.

[46] B. Young, K.J.R. Rasmussen, Shift of effective centroid of channel columns, J. Struct. Eng., ASCE 125 (2) (1999) 524–531.

[47] Y. Zhang, C. Wang, Z. Zhang, Tests and finite element analysis of pin-ended channel columns with inclined simple edge stiffeners, J. Constr. Steel Res. 63 (2007) 383–395.